SUPPORTING INFORMATION

Time-Gated FRET and DNA-Based Photonic Molecular Logic Gates: AND, OR, NAND and NOR

Melissa Massey[1], Igor L. Medintz[2], Mario G. Ancona[3], W. Russ Algar[1,*]

[1] Department of Chemistry, University of British Columbia,
2036 Main Mall, Vancouver, British Columbia, V6T 1Z1, Canada.

[2] Center for Bio/Molecular Science and Engineering, Code 6900

[3] Electronic Science and Technology Division, Code 6876
U.S. Naval Research Laboratory, 4555 Overlook Ave. SW,
Washington, DC, 20375, United States of America

***Corresponding author:** algar@chem.ubc.ca (WRA). Tel: 1-604-822-2464.

Table of Contents

Additional Experimental Details

Labeling oligonucleotides. Oligonucleotides (see Table S1 on pg. S8 for sequences) were obtained from Integrated DNA Technologies (Coralville, IA) with thiol linkers (protected as a disulfide) and amine linkers to enable labeling in-house. Thiol-terminated oligonucleotides were labeled at their 5' and/or 3' termini (see Table S1 on pg. S8) with A546 maleimide for use in most logic gates, and selected sequences were labeled with A488 maleimide for two-color applications. Amine-terminated oligonucleotides were labeled at either their 3' terminus, 5' terminus, or at an internal amine linker with Lumi4-Tb-NHS (see Table S1 for positions). When dual labeling was required, dye-labeling at a thiol linker was done before labeling with Tb at an amine linker. Oligonucleotide blocking sequences with terminal IabFQ labels were directly obtained from Integrated DNA Technologies.

As-received oligonucleotides with protected thiol linkers were first reduced to yield reactive thiol groups using tris(2-carboxyethyl)phosphine (TCEP) as a reducing agent. Oligonucleotides (50 nmol) were first dissolved in 92 μL of water (UltraPure, Amresco, Solon, OH) and 8 μL of an aqueous 150 mM TCEP solution was added. The solution was mixed for 1 h, after which time the TCEP was removed using a NAP-10 size exclusion column (GE Healthcare, Baie-D'Urfé, QC, Canada) with elution using 4-(2-hydroxyethyl)-1-piperazineethanesulfonic acid (HEPES) buffer (100 mM, 50 mM NaCl, pH 7). The eluate (600 μL) was mixed with 20 μL of dye dissolved in DMSO (12.5 mg/mL). The reaction was mixed overnight and the labeled oligonucleotides were then purified using Bio-Gel P-4 (Bio-Rad, Mississauga, ON, Canada) size exclusion chromatography with an eluent of triethylammonium acetate buffer (0.2 M TEAA, pH 7). The DNA:dye ratios were verified using UV-visible absorption spectrophotometry. Purified samples were dried in a vacuum centrifuge.

To label oligonucleotides with Tb (whether initially unlabeled or dye-labeled), a 5 mg/mL stock solution of Lumi4-Tb-NHS was prepared by dissolving ~1 mg of Lumi4-Tb-NHS in 200 μL of DMSO. Oligonucleotides were dissolved in 150 μL of borate buffer (100 mM, pH 8.5) and 50 μL of DMSO was added to the solution. To this mixture, 100 μL of the Lumi4-Tb-NHS stock solution was added so that the final solvent was a 1:1 mixture (v/v) of DMSO and buffer. The

reaction was mixed overnight and purified using size exclusion chromatography (Bio-Gel P-4) with 0.2 M TEAA as the eluent. DNA:Tb or DNA:dye:Tb ratios were verified using UV-visible absorption spectrophotometry. Purified samples were dried in a vacuum centrifuge until required for use.

Calculation of Förster distances. Spectral overlap integrals, J, and Förster distances, R_0, for the Tb-A546, Tb-IabFQ, and A546-IabFQ FRET pairs were calculated using eqns. S1 and S2, where $I_D(\lambda)$ is the wavelength-dependent emission intensity of the donor, $\varepsilon_A(\lambda)$ is the wavelength-dependent molar absorption coefficient of the acceptor (ε_{max} = 112 000 M^{-1} cm^{-1} for A546 and ε_{max} = 38 200 M^{-1} cm^{-1} for IabFQ), n = 1.34 is the refractive index of the medium, κ^2 is the orientation factor (approximated as 2/3), and Φ_D is the quantum yield of the donor (0.77 for Tb and 0.79 for A546).

$$J = \frac{\int I_D(\lambda)\varepsilon_A(\lambda)\lambda^4 d\lambda}{\int I_D(\lambda)d\lambda} \tag{S1}$$

$$R_0^6 = (8.79\times10^{-28} mol)n^{-4}\Phi_D\kappa^2 J \tag{S2}$$

Competitive FRET calculations. Figure 1C in the main text shows the percentage of Tb-to-IabFQ FRET events (*i.e.* dark or "false" state) *versus* Tb-to-A546 FRET events (*i.e.* bright or "true" state) for different separation distances between the Tb and IabFQ and Tb and A546. The general rate of FRET is given by Eqn. S3, where k_{Tb} is the intrinsic relaxation rate for the Tb donor, $R_{0,\,Tb\text{-}A}$ is the Förster distance for the Tb donor-dye acceptor pair, and $r_{Tb\text{-}A}$ is the separation distance between the Tb and dye acceptor.

$$k_{FRET} = k_{Tb}\left(\frac{R_{0,Tb\text{-}A}}{r_{Tb\text{-}A}}\right)^6 \tag{S3}$$

The FRET efficiencies for the Tb-to-IabFQ pathway in Figure 1A-iii is given by Eqn. S4:

$$E_{Tb\text{-to-}IabFQ} = \frac{k_{Tb}\left(\frac{R_{0,Tb\text{-}IabFQ}}{r_{Tb\text{-}IabFQ}}\right)^6}{k_{Tb} + k_{Tb}\left(\frac{R_{0,Tb\text{-}IabFQ}}{r_{Tb\text{-}IabFQ}}\right)^6 + k_{Tb}\left(\frac{R_{0,Tb\text{-}A546}}{r_{Tb\text{-}A546}}\right)^6} \tag{S4}$$

The total efficiency of FRET, accounting for both the Tb-to-IabFQ and Tb-to-A546 pathways is given by Eqn. S5:

$$E_{\text{Total}} = \frac{k_{\text{Tb}}\left(\frac{R_{0,\text{Tb-IabFQ}}}{r_{\text{Tb-IabFQ}}}\right)^6 + k_{\text{Tb}}\left(\frac{R_{0,\text{Tb-A546}}}{r_{\text{Tb-A546}}}\right)^6}{k_{\text{Tb}} + k_{\text{Tb}}\left(\frac{R_{0,\text{Tb-IabFQ}}}{r_{\text{Tb-IabFQ}}}\right)^6 + k_{\text{Tb}}\left(\frac{R_{0,\text{Tb-A546}}}{r_{\text{Tb-A546}}}\right)^6} \quad \text{(S5)}$$

The fraction of FRET events, X, that are Tb-to-IabFQ FRET and lead to a dark output is therefore given by Eqn. S6:

$$\text{X}_{\text{Tb-to-IabFQ}} = \frac{E_{\text{Tb-to-IabFQ}}}{E_{\text{Total}}} = \frac{\left(\frac{R_{0,\text{Tb-IabFQ}}}{r_{\text{Tb-IabFQ}}}\right)^6}{\left(\frac{R_{0,\text{Tb-IabFQ}}}{r_{\text{Tb-IabFQ}}}\right)^6 + \left(\frac{R_{0,\text{Tb-A546}}}{r_{\text{Tb-A546}}}\right)^6} \quad \text{(S6)}$$

Eqn. S6 was used to calculate the data in Figure 1C.

Contrast and threshold values. The contrast between "true" and "false" states was calculated as the ratio of the time-gated A546 PL intensity for the lowest-intensity "true" state divided by that for the highest-intensity "false" state. The threshold for switching from a "false" to "true" output signal (AND, OR gates) was the average time-gated A546 PL intensity for the highest-intensity "false" state plus five sample standard deviations. Considering the sample size and Student's *t* distribution, this threshold corresponds to ~95% confidence. Analogously, the threshold for switching from "true" to "false" output (NAND, NOR gates) was the average time-gated A546 PL intensity for the lowest-intensity "true" state minus five sample standard deviations.

Higher contrast between "true" and "false" states is likely to translate into greater Boolean sensitivity and specificity, where the former is CT/(CT+IF) and the latter is CF/(CF+IT), where CT is the frequency of correct "true" measurements, IF is the frequency of incorrect "false" measurements, CF is the frequency of correct "false" measurements, and IT is the frequency of incorrect "true" measurements. A higher contrast is also likely to translate into lower (AND, OR) or higher (NOR, NAND) thresholds for switching between "true" and "false" output, which will enable the logical detection of smaller amounts of input (*e.g.*, when the logic gate is in excess versus the inputs).

Statistical fitting of calibration curves. Eqn. 1 in the main text is reproduced below as Eqn. S7. This equation is applicable to a situation where a logic gate is challenged with a range of equivalents of one or both of its inputs as (χ_1, χ_2), where $0 \leq \chi_1, \chi_2 \leq 1$. The parameters *D*, *C*, *B*, and *A* are derived from the relative time-gated dye PL intensity for the (0,0), (1,0), (0,1), and (1,1) cases, respectively. *F* and *K* are fitting parameters to account for the arbitrary units of PL intensity. When fitting data, the values of *F* and *K* were kept constant between the experiments with (0,χ_2), (χ_1,0), and (χ_1,χ_2).

$$I_{A546} = F\left[A\chi_1\chi_2 + B(1-\chi_1)\chi_2 + C\chi_1(1-\chi_2) + D(1-\chi_1)(1-\chi_2)\right] + K \quad \text{(S7)}$$

Eqn. S7 was used for fitting the experiments (0,χ_2) and (χ_1,0); however, Eqn. S8 was used for fitting the experiments (χ_1,χ_2). The difference between Eqn. S7 and Eqn. S8 is that the latter uses the coefficient *E*, which is the arithmetic average of *B* and *C*. That is, $E = 0.5(B + C)$. This simplification was sufficient for fitting the (χ_1,χ_2) experiments. *F, K*, *A* and *D* were kept constant between Eqn. S7 and Eqn. S8.

$$I_{A546} = F\left[A\chi_1\chi_2 + E\left[(1-\chi_1)\chi_2 + \chi_1(1-\chi_2)\right] + D(1-\chi_1)(1-\chi_2)\right] + K \quad \text{(S8)}$$

Eqns. S7–S8 assume tight binding. That is, a very large equilibrium constant that favors toehold-mediated strand displacement of each blocking sequence with replacement by the corresponding input sequences, limited only by the number of equivalents of each input available. The mole fractions, χ_n, of each input (relative to the logic gate) represent the probability that the n^{th} input hybridizes to a logic gate. In order, the mole fraction products in Eqn. S8 are thus the probabilities that the two required inputs hybridize to the same logic gate, that the two inputs hybridize to different logic gates, and that a logic gate has no hybridized inputs. Although a simple explanation for the shape of the calibration curves, Eqns. S7–S8 are not useful for more than one equivalent of the input sequences.

Normalization of kinetic traces. Instrument drift or other sources of drift are often observed during kinetic measurements. Relative drift was always less than 25% in our kinetic experiments. To adjust for changes in PL intensity that were unrelated to the addition of oligonucleotide inputs, kinetic traces were normalized to control samples (no added inputs) that were measured in parallel. Shorter timescale (< 1 h) kinetic data often did not need to be corrected for drift.

The trend in the drift for the control sample PL intensities was generally linear. The drift was fit with a line of the form $I_X = mt + b$ where I_X is the time-gated PL intensity of X = Tb or A546, t is time, m is the slope, and b is the intercept. Each raw PL intensity data point, I_X, (for all samples) was divided by the expected value for the line at the corresponding time, t, then multiplied by the average value for the line across all times. This method recovers the original units and magnitude of the PL intensity and retains the noise/variation in the signal while eliminating systematic drift.

Table S1. Oligonucleotide sequences and label positions for logic gates.

Gate	Role	Sequence
AND-I	Template	A546–5′–TAG GCT CAG CTG GCT GGT T–(Tb)–T CGT GGT GAT CGC GTC CTT–3′–A546
	Block 1	IabFQ–5′–ACC AGC CAG CTG A–3′
	Block 2	5′–CGC GAT CAC CAC G–3′–IabFQ
	Input 1	5′–ACC AGC CAG CTG AGC CTA–3′
	Input 2	5′–AAG GAC GCG ATC ACC ACG–3′
AND-II	Template	5′–TAG GCT CAG CTG GCT GGT AAG GAC GCG ATC ACC ACG CAG TGA AGC GGT ACA TAG G–3′
	Reporter	A546–5′–CGT GGT GAT CGC GTC CTT–3′–Tb
	Block 1	IabFQ-5′–ACC AGC CAG CTG A–3′
	Block 2	5′–GTA CCG CTT CAC TG–3′–IabFQ
	Input 1	5′–ACC AGC CAG CTG AGC CTA–3′
	Input 2	5′–CCT ATG TAC CGC TTC ACT G–3′
OR	Template	5′–TAG GCT CAG CTG GCT GGT AAG GAC GC***T*** ATC ACC–3′
	Block	IabFQ–5′–ACC AGC CAG CTG A–3′
	Reporter	A546–5′–CGT GGT GAT CGC GTC CTT–3′–Tb
	Reporter	A488–5′–CGT GGT GAT CGC GTC CTT–3′–Tb
	Input 1	5′–ACC AGC CAG CTG AGC CTA–3′
	Input 2	5′–AAG GAC GCG ATC ACC ACG–3′
NAND	Template	5′–TAG GCT CAG CTG GCT GGT–(Tb)–CGT GGT GAT ***C***GC GTC CTT–3′
	Block	5′– ACG TAC CAG CCA GCT GA–3′
	Reporter	A546–5′– AAG GAC GCT ATC ACC–3′
	Input 1	5′– ACC AGC CAG CTG AGC CTA–3′
	Input 2	5′– AAG GAC GCG ATC ACC ACG–3′
NOR	Template	5′–TAG GCT CAG CTG GCT GGT AAG GAC GC***T*** ATC ACC–3′
	Antenna	Tb–5′–ACC AGC CAG CTG A–3′
	Reporter	A546–5′–CGT GGT GAT CGC GTC CTT–3′
	Input 1	5′–ACC AGC CAG CTG AGC CTA–3′
	Input 2	5′–AAG GAC GCG ATC ACC ACG–3′
OR 2. col. (Fig. S3B)	Template	5′–CAG TGA AGC GGT ACA TAG GAC CAG CCA ***T***CT GAG C–3′
	Block 3	IabFQ–5′–CCT ATG TAC CGC T–3′
	Reporter	A488–5′–TAG GCT CAG CTG GCT GGT–3′–Tb
	Input 1	5′–ACC AGC CAG CTG AGC CTA–3′
	Input 3	5′–CCT ATG TAC CGC TTC ACT G–3′

Tb = Lumi4-Tb cryptate; A488 = Alexa Fluor 488; A546 = Alexa Fluor 546; IabFQ = Iowa Black Dark Quencher.

Additional Results and Discussion

Full emission spectra for the logic gates. Figure S1 below shows the full time-gated PL emission spectra for each of the AND-I, AND-II, OR, NOR and NAND logic gates for the (0,0), NC, (1,0), (0,1), and (1,1) input states. NC refers to challenging the gates with a non-complementary sequence. The excitation wavelength was 355 nm, which was ideal for the Tb donor. The "true" output signal is from time-gated FRET-sensitized PL from the A546 acceptor dye and was measured at its PL maximum of 572 nm. The Tb donor had a minimum in its PL signal at the PL maximum for the A546 acceptor, thereby providing good contrast between "true" and "false" output signals.

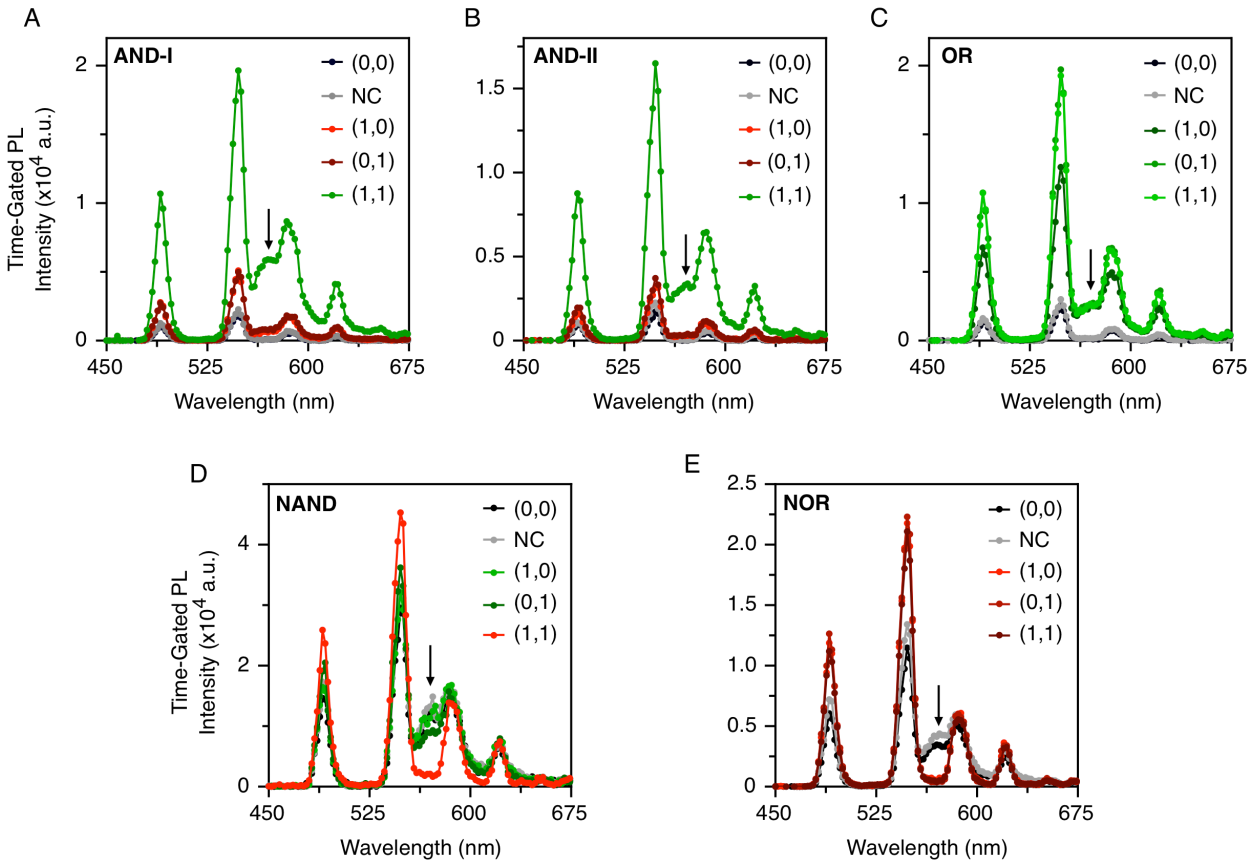

Figure S1. Time-gated PL emission spectra for the **(A)** AND-I, **(B)** AND-II, **(C)** OR, **(D)** NAND, and **(E)** NOR logic gates. Each plot shows spectra for the (0,0), NC, (1,0), (0,1), and (1,1) input states. The arrow indicates the wavelength (572 nm) used for simple measurements of A546 PL intensity.

Extended calibration curves with AND gates. Figure S2 shows calibration curves for the AND-I and AND-II logic gates when challenged with more than one equivalent of both input sequences. As seen in the figures, the output of the logic gates in response to the (1,1) input are non-ideal in that a "soft" saturation is observed for concentrations above one equivalent. Similar behavior in strand displacement reactions has been observed by others,[1-2] and the main reasons implicated are a finite equilibrium constant, kinetic limitations, and synthesis errors (the solid-phase synthesis error rate is estimated at 0.6-0.8% per base). It is also possible that the behavior is affected by unintended interactions between DNA strands or between the DNA and the dyes or Tb. Because our structures are much simpler than those of refs.[1-2], it seems reasonable to assume that the effects of synthesis errors and of unwanted interactions are small. Our experiments also indicated that there was sufficient time to reach equilibrium prior to measurements and so kinetics need not be considered. On this basis, we consider a simple equilibrium model to rationalize the "soft" saturation of the AND gates.

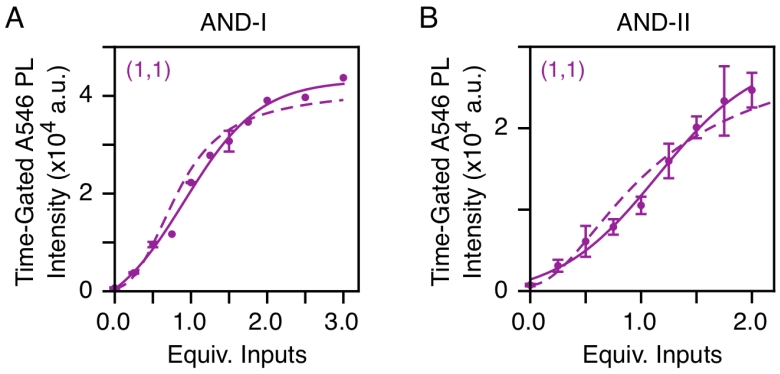

Figure S2. Extended calibration curves for the **(A)** AND-I and **(B)** AND-II gates. The solid lines are empirical trend lines whereas the dashed lines are fits to the equilibrium model.

For the equilibrium model, let $t_{(i,j)}$ denote the template, t, with i and j labeling the two input binding sites and being 0 initially (block strand hybridized) and becoming 1 when a strand displacement occurs (input strand hybridized). The possible reactions are summarized by Eqns. S9–S12, where oligonucleotides are denoted as in Figures 2 and 3.

$$t_{(0,0)} + I1 \underset{k_{-1}}{\overset{k_1}{\rightleftarrows}} t_{(1,0)} + b1 \tag{S9}$$

$$t_{(0,0)} + I2 \underset{k_{-2}}{\overset{k_2}{\rightleftarrows}} t_{(0,1)} + b2 \tag{S10}$$

$$t_{(0,1)} + I1 \underset{k_{-1}}{\overset{k_1}{\rightleftarrows}} t_{(1,1)} + b1 \tag{S11}$$

$$t_{(1,0)} + I2 \underset{k_{-2}}{\overset{k_2}{\rightleftarrows}} t_{(1,1)} + b2 \tag{S12}$$

The reactions at each arm of the template are assumed to occur independently so that the reaction constants can be assumed to be the same regardless of which strand hybridizes first. Defining the various concentrations (in equivalents) as $\chi_c \equiv [C]/[t_{total}]$ and the equilibrium constants as $K_m \equiv k_m/k_{-m}$, equations S13–S17 result:

$$\frac{K_1 \chi_{I1}}{\chi_{b1}} = \frac{\chi_{t_{10}}}{\chi_{t_{00}}} = \frac{\chi_{t_{11}}}{\chi_{t_{01}}} \tag{S13}$$

$$\frac{K_2 \chi_{I2}}{\chi_{b2}} = \frac{\chi_{t_{01}}}{\chi_{t_{00}}} \tag{S14}$$

$$\chi_{I1} + \chi_{t_{10}} + \chi_{t_{11}} = \chi_{I1}^{total} \tag{S15}$$

$$\chi_{I2} + \chi_{t_{01}} + \chi_{t_{11}} = \chi_{I2}^{total} \tag{S16}$$

$$\chi_{b1} + \chi_{t_{00}} + \chi_{t_{01}} = \chi_{b2} + \chi_{t_{00}} + \chi_{t_{10}} = \chi_{t_{00}} + \chi_{t_{01}} + \chi_{t_{10}} + \chi_{t_{11}} = 1 \tag{S17}$$

These are 8 equations with 8 unknowns. The value of t_{11} is proportional to the (1,1) output of the AND gate. A full solution is readily obtained, however, we consider only the special case when $K_1 = K_2 \equiv K$ and as in the experiments with $\chi_{I1}^{total} = \chi_{I2}^{total} \equiv \chi_I^{total}$. With these assumptions one can show that the algebra reduces to Eqn. S18:

$$\left(\frac{K-1}{K}\right) {\chi_{b1}}^2 - \chi_{b1}\left(1 + \chi_I^{total}\right) + \chi_I^{total} = 0 \text{ where } \chi_{t_{11}} = {\chi_{b1}}^2 \tag{S18}$$

These equations are quadratics and so reduce to closed-form solutions that were used to fit the data in Figure S2 with scaling for the arbitrary units of the data. The parameter values were $K \sim 10$ for AND-I and $K \sim 3$ for AND-II. Such small values of K are surprising for strand displacement situations and suggest that this is not the entire explanation for the soft saturation.

Multiplexed logic. Figure 7 in the main text summarizes two different two-color logic experiments: (1) an experiment with two common inputs for the AND-I gate (A546 dye) and an OR gate (A488 dye); and (2) an experiment with only one common input for the AND-I gate (A546 dye) and an OR gate (A488 dye), where the second input for each logic gate was exclusive to that gate. The FRET-sensitized time-gated PL from the A488 and A546 was detected at 520 nm and 572 nm, respectively, with minimal background from the Tb PL. Figure S3 shows full spectra and close-up views of the dye PL regions for the experiments in Figure 7.

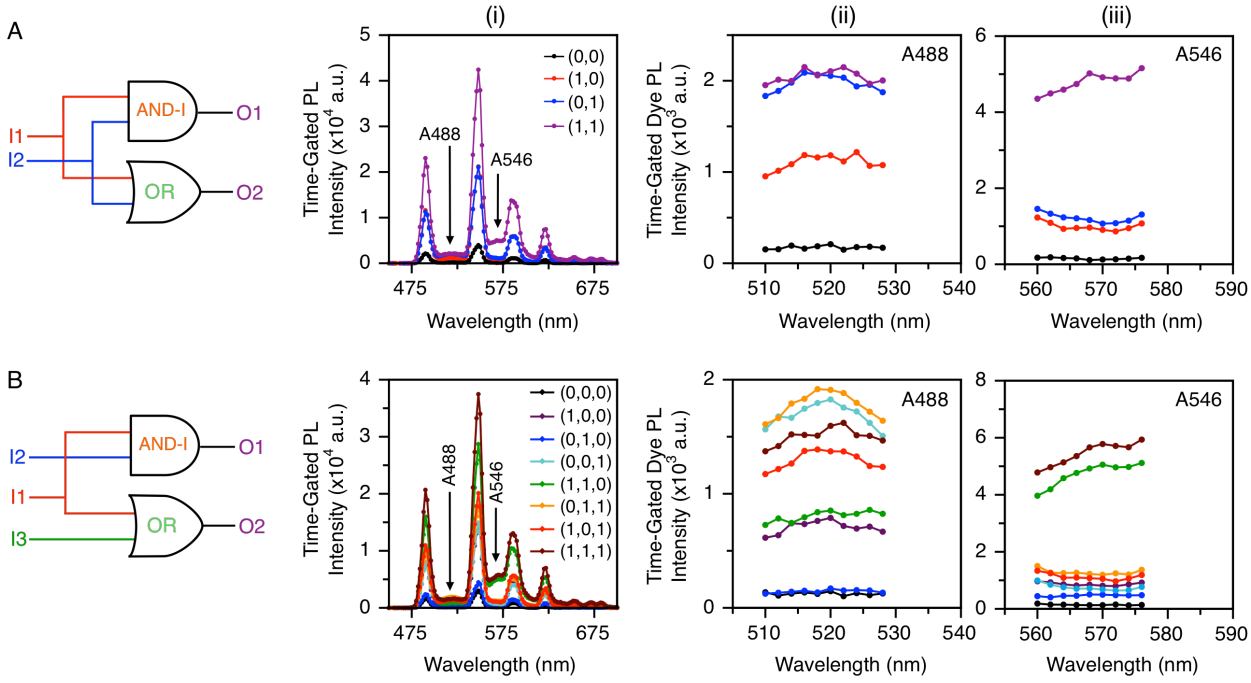

Figure S3. Full time-gated PL spectra (i) and close-up on the spectral regions for OR-A488 (ii) and AND-I-A546 (iii) emission for the multiplex logic experiments in Figure 7. **(A)** Two-input, two-color AND-I and OR combination. **(B)** Three-input, two-color AND-I and OR combination.

Logic gate performance in serum. Figure S4 summarizes the overall performance of the AND-I, AND-II, OR, NOR, and NAND logic gates in ~90% serum (data reproduced from Figures 2B–6B). Logic gates in serum were challenged with two equivalents of one or both of the target inputs, with a gate concentration of 0.25 μM. When the time-gated A546 PL was normalized to the maximum output for the (1,1) input state, analytically useful contrast and thresholds were retained, albeit reduced compared to a simple buffer matrix.

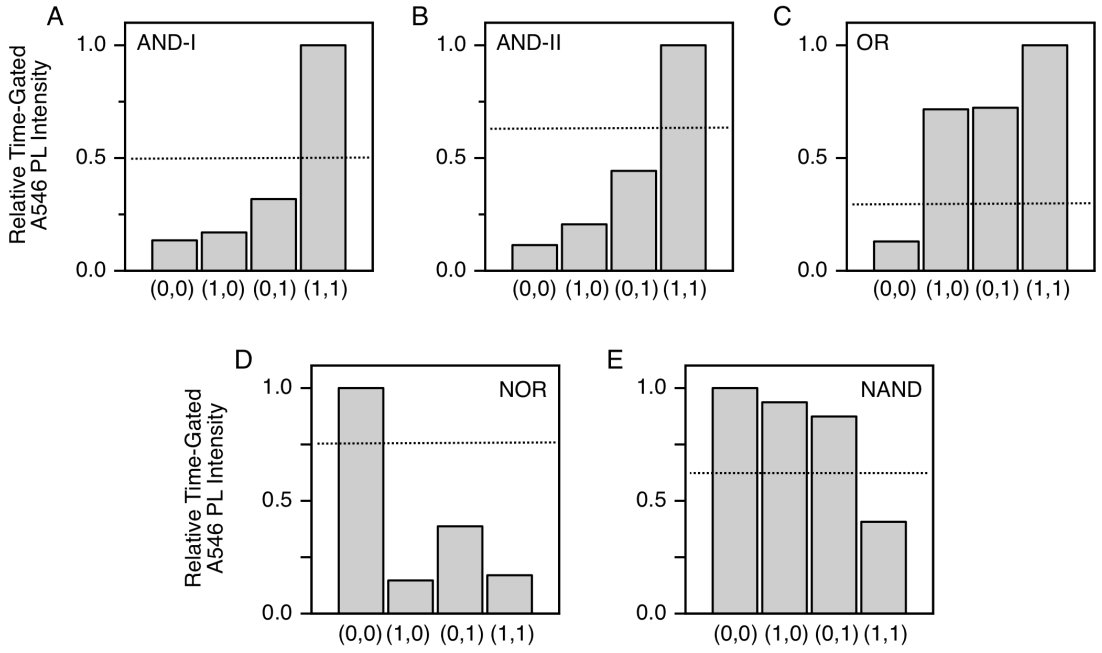

Figure S4. Relative time-gated A546 PL intensity when the **(A)** AND-I, **(B)** AND-II, **(C)** OR, **(D)** NOR and **(E)** NAND gates were challenged with two equivalents of inputs in 90% v/v bovine serum (normalized to mimic truth table-like output). The dotted lines are qualitative thresholds.

Figure S5 shows the AND-I gate performance in 50% and 90% v/v serum when the lag time and integration time for time-gated measurements were increased from 1000 μs each to 2000 μs each. When normalized to the maximum output for the (1,1) input state, there was only a very small decrease in the contrast versus the NC, (1,0), and (0,1) states with an increasing percentage of serum. (NC refers to addition of a non-complementary sequence.) This result suggests that optimization of time-gated measurement settings can lead to very robust measurements in serum matrices. Such optimization will be explored in future work.

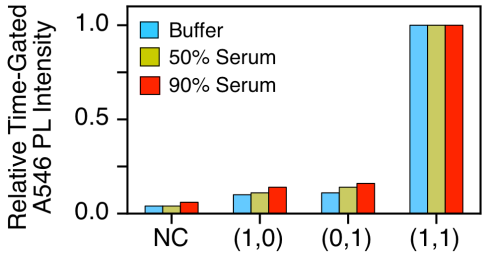

Figure S5. Relative time-gated A546 PL intensity when the AND-I gate is challenged with an equivalent of inputs in buffer, 50% v/v bovine serum, and 90% v/v bovine serum (normalized to mimic truth table-like output). Measurement of the time-gated FRET-sensitized A546 PL shifts signal acquisition outside of the time window associated with scattering and autofluorescence from the serum matrix. The lag time and the integration time were both 2000 μs (cf. 1000 μs in other experiments).

Longer oligonucleotide inputs with AND-I. Figure S6 shows the performance of the AND-I gate with target inputs that were longer (48 nt) than the portion of the gate template sequence to which they hybridized (18 nt). The performance with equal length (18 nt) target inputs is shown for comparison. The 48 nt targets had the same 18 nt complementary sequence to the template arms but also had flanking ends that were 15 nt in length and not complementary with the template. The performance of the AND-I logic gate with the two lengths of target input was nearly indistinguishable, and a threshold of ≤ 0.17 was possible with the 48 nt inputs.

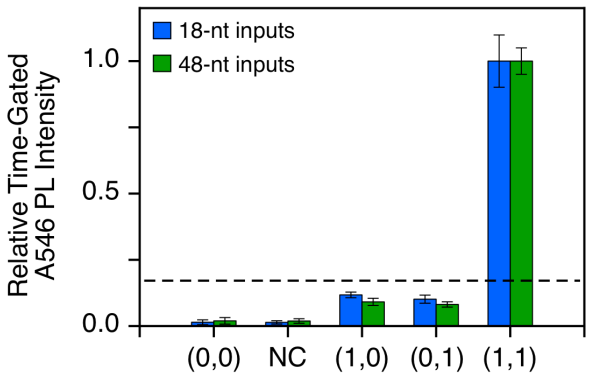

Figure S6. Relative time-gated A546 PL intensity for the AND-I gate when challenged with an equivalent of one or both inputs (normalized to mimic truth table-like output) when the inputs were either 48 nt in length or 18 nt in length.

Optimization of OR gate design. The first OR gate design that was tested was a derivative of AND-I. Analogous to AND-I, the "OR-I" gate consisted of two 19 nt template arms joined through an internal amine linker that was labeled with Tb. The 3' and 5' termini of the probe were labeled with A546. The difference between OR-I and AND-I was the nature of the blocking sequence(s). With OR-I, the blocking sequence also consisted of two arms, each 14 nt in length to leave 5 nt toeholds at opposite ends of the OR-I gate. The two arms were joined by an internal amine linker that was labeled with a Black Hole Quencher (BHQ) dye. Each arm of the blocking sequence included two mismatches to destabilize the hybridization. When both arms of the blocking sequences were hybridized to the OR-I template, as the (0,0) state, the hybrid was stable, and the BHQ efficiently quenched the Tb. Ideally, when one target hybridized and displaced one arm of the blocking sequence, as either a (1,0) or (0,1) input state, the remaining arm was too unstable to remain hybridized. The blocking sequence then dissociated from the probe with recovery of both the time-gated Tb emission and the time-gated FRET-sensitized A546 emission. The outcome would be analogous when both targets are added as the (1,1) input state.

In practice, the OR-I design did not provide high contrast, as shown in Table S2. One possible explanation is that the blocking sequence was not fully displaced, resulting in a decrease in Tb-to-BHQ efficiency but not complete loss of this competitive quenching pathway. A second explanation was that the loss of rigid double-stranded structure lead to some spontaneous association between the Tb and A546, as we have reported previously.[3] This latter explanation is more likely given the low predicted melt temperature for each arm of the blocking sequence and the ineffectiveness of changes in buffer ionic strength in optimizing the signaling. Attempts were made to "splint" the single stranded arms with short oligonucleotides after displacement of the blocking sequence; however, these attempts were unsuccessful. The apparent need to maintain sufficient double-stranded structure between the Tb and A546 was thus an important factor in designing not only the OR gate in the main text, but also all other logic gates.

Table S2. Experimental truth tables as relative time-gated A546 PL intensity for OR logic gate designs.

	Relative time-gated A546 PL Intensity			
Logic Gate	*(0,0)*	*(1,0)*	*(0,1)*	*(1,1)*
OR-I	0.06	0.35	0.25	1.0
OR-3-1*	0.11	0.96	0.90	1.0
OR-2-2	0.10	0.90	0.89	1.0
OR-1-3	0.08	0.82	0.33	1.0
OR-0-4	0.08	0.72	0.45	1.0

* The selected OR logic gate design that was reported in the main text. Near-ideal response for one input is highlighted in green. Poor response is highlighted in red and moderate response is highlighted in beige.

The OR gate in the main text is a design that incorporates a 3 nt toehold at the 5′ terminus of the Tb- and A546-labeled reporter oligonucleotide and a centrally-located 1 base pair mismatch (bpm). Strand displacement kinetics are known to increase with increasing toehold length,[4-5] so the purpose of the 1 bpm was to somewhat destabilize hybridization and help facilitate displacement with a shorter toehold. The more detailed shorthand notation for this logic gate is OR-3-1, where the first number is the toehold length and the second number is the number of mismatches incorporated along the length of the reporter. The OR-3-1 gate was selected from a total of four related designs: OR-3-1, OR-2-2, OR-1-3, and OR-0-4. In the case of multiple mismatches, the mismatches were distributed approximately equidistant along the reporter sequence. Table S2 summarizes the experimental truth table for the OR gates in terms of the relative time-gated A546 PL intensity. Both OR-3-1 and OR-2-2 designs provided good contrast and the most consistency between the (0,1), (1,0), and (1,1) input states. The OR-1-3 and OR-0-4 designs showed comparatively modest increases in time-gated A546 PL for the (0,1) input state, which, as an input, was dependent on the toehold that was being varied in length and paired with the mismatch. Given the similar contrast between OR-2-2 and OR-3-1, the latter was selected as the final design because of the faster displacement kinetics associated with the 3 nt toehold. Figure S7 shows the kinetic response of the OR-2-2 gate versus the OR-3-1 gate.

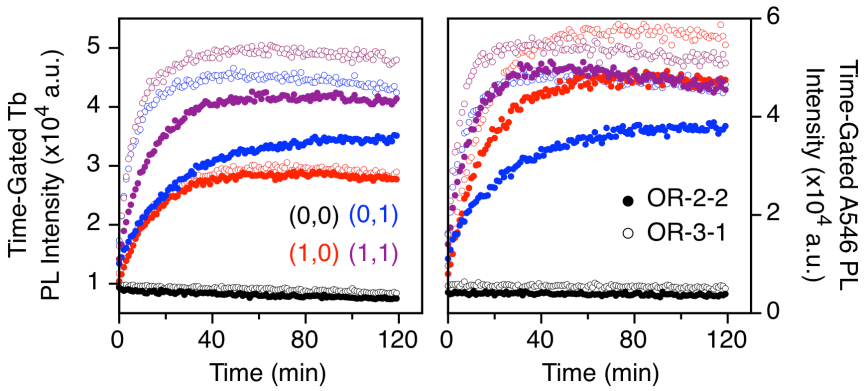

Figure S7. Kinetic traces of the time-gated Tb and A546 PL intensity for the OR-2-2 gate (solid circles) versus the OR-3-1 gate (open circles) when challenged with one or both inputs. The kinetics were slower for the OR-2-2, particularly with the (0,1) input, which utilized the toehold that was varied in length.

Three-input AND gate. Figure S8 shows the design of a three-input AND gate. Sequences are listed in Table S3. The design relied upon a template labeled with Tb and A546 with three toeholds for strand displacement by three inputs, where only one of the toeholds was open and the other two toeholds were hidden[6] by blocking sequences. The first input (I1) displaced the first block (b_1) and exposed the second toehold, which then allowed I2 to bind and displace the second block (b_2). In turn, a third toehold was exposed, which allowed I3 to bind and displace the third block. The third block was labeled at both termini with IabFQ, quenching the Tb and A546. Displacement of the third block led to efficient Tb-to-A546 FRET and a "true" output manifested as a large increase in the time-gated A546 PL intensity. Figure S9 shows an experimental truth table for the three-input AND gate in terms of the relative time-gated A546 PL intensity. The threshold for "true/false" was 0.13 for a 0.1 μM logic gate concentration challenged with 5 equivalents of target oligonucleotide inputs.

The strategy of cascading a series of hidden and revealed toeholds is, in principle, suitable for designing AND gates with any arbitrary number of inputs, whether it be two inputs, three inputs, or even more. (Practical limits may be imposed by factors such as displacement kinetics, template oligonucleotide length, *etc.*) The FRET system associated with the final blocking sequence will provide signaling contrast provided that each toehold (except the first) can be

effectively hidden. The strategy can also be effective for designing NAND logic gates with multiple inputs (*vide infra*). Future work will be required to develop strategies for three-input OR and NOR logic gates.

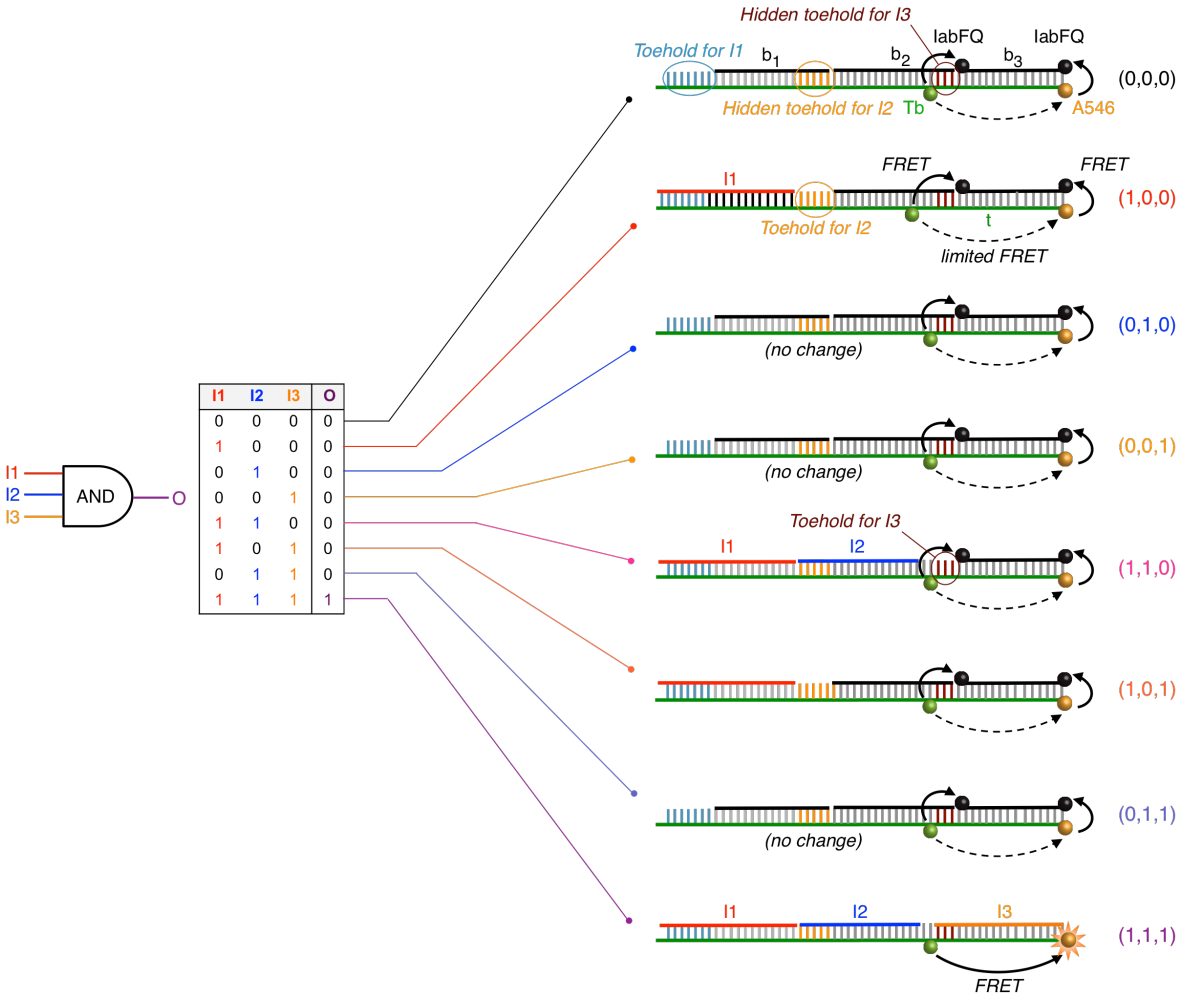

Figure S8. Truth table and DNA structures for a three-input AND gate. The template (t), blocking (b_1, b_2, b_3), and input (I1, I2, I3) oligonucleotides are labeled. Tb, A546, and labFQ are also labeled. Toeholds for strand displacement by the inputs are circled. Efficient FRET is shown as a solid arrow. Weak but non-zero FRET is shown as a dashed arrow.

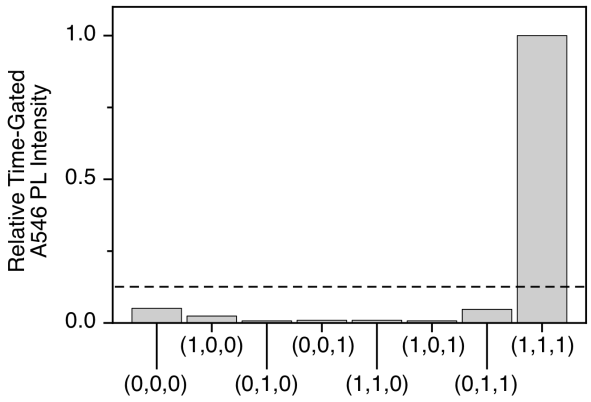

Figure S9. Experimental truth table as the relative time-gated A546 PL intensity when the three-input AND gate was challenged with different combinations of its three inputs. The "false/true" threshold is shown as the dashed line.

In the three-input AND logic gate design, the third blocking oligonucleotide was labeled at both of its termini with IabFQ, and was thus able to quench both the Tb donor and A546 acceptor. Strand displacement of the third block led to a very large increase in the time-gated A546 PL intensity. Initial experiments also tested a three-input AND gate with a single IabFQ label at the 5′ terminus of third block. In this position, the IabFQ would exert a large quenching effect on the A546 but a much lower quenching effect on the Tb. Figure S10 shows the head-to-head performance of the three-input AND gate using the single IabFQ label versus the double IabFQ labels. With the single label, the "false/true" threshold was ~0.6; with the double label the threshold was < 0.3.

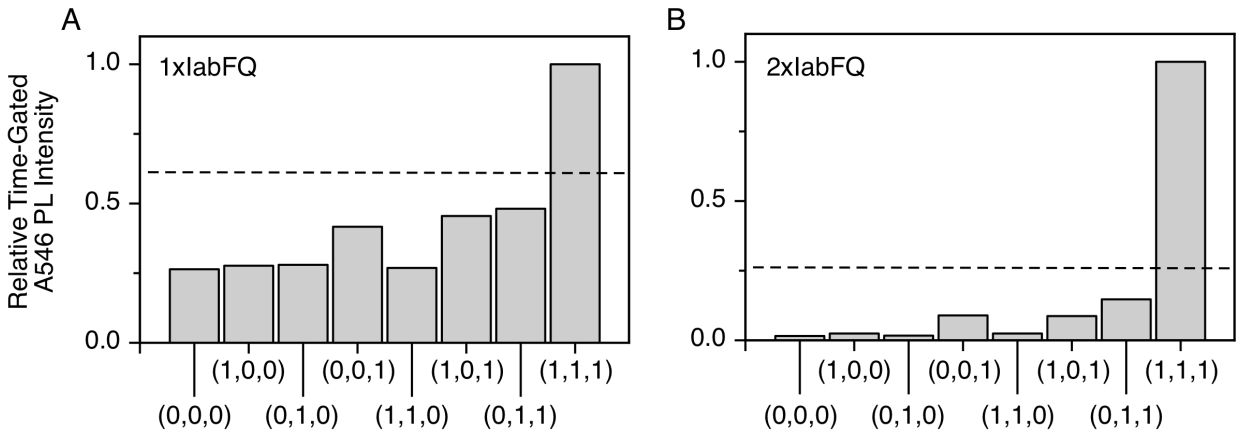

Figure S10. Comparison of the three-input AND gate when the third block was **(A)** singly labeled at its 5' terminus with IabFQ versus **(B)** dual-labeled with IabFQ at both termini. Experimental truth tables as the relative time-gated dye A546 PL intensity when the three-input AND gates were challenged with different combinations of its three inputs.

Table S3. Oligonucleotide sequences and label positions for three-input AND and NAND gates.

Role	**Sequence**
Template	5′–C AGT GAA GCG GTA CAT AGG TAG GCT CAG CTG GCT GGT–Tb–CGT GGT GAT CGC GTC CTT–3′–A546
Block 1	5′–GCC TAC CTA TGT ACC GC–3′
Block 2	5′–ACG T AAC CAG CCA GCT GA–3′
Block 3 (AND)	IabFQ–5′–AAG GAC GCG ATC ACC–3′–IabFQ
Block 3 (NAND)	A546–5′–AAG GAC GCG ATC ACC–3′
Input 1	5′–CCT ATG TAC CGC TTC ACT G–3′
Input 2	5′–ACC AGC CAG CTG AGC CTA–3′
Input 3	5′–AAG GAC GCG ATC ACC ACG–3′

Three-input NAND gate. The strategy for the three-input AND gate was also evaluated for designing a NAND gate with three inputs. As shown in Figure S11, the gate design was identical to the three-input AND gate except that the A546 was removed from the template strand and placed on the third blocking sequence at its 5' terminus. Displacement of the third block in response to the (1,1,1) input state led to loss of Tb-to-A546 FRET with a "false" output generated as a decrease in the time-gated FRET-sensitized A546 PL intensity. Figure S12 shows

the performance of the three-input NAND gate, which had a "true/false" threshold of ~0.6 for a 0.1 μM concentration of logic gate challenged with 10 equivalents of target oligonucleotide inputs. The lower contrast versus the three-input AND gate suggests that these hidden-toehold systems may require significant optimization. Additional future work will also be required to develop strategies for three-input OR and NOR logic gates.

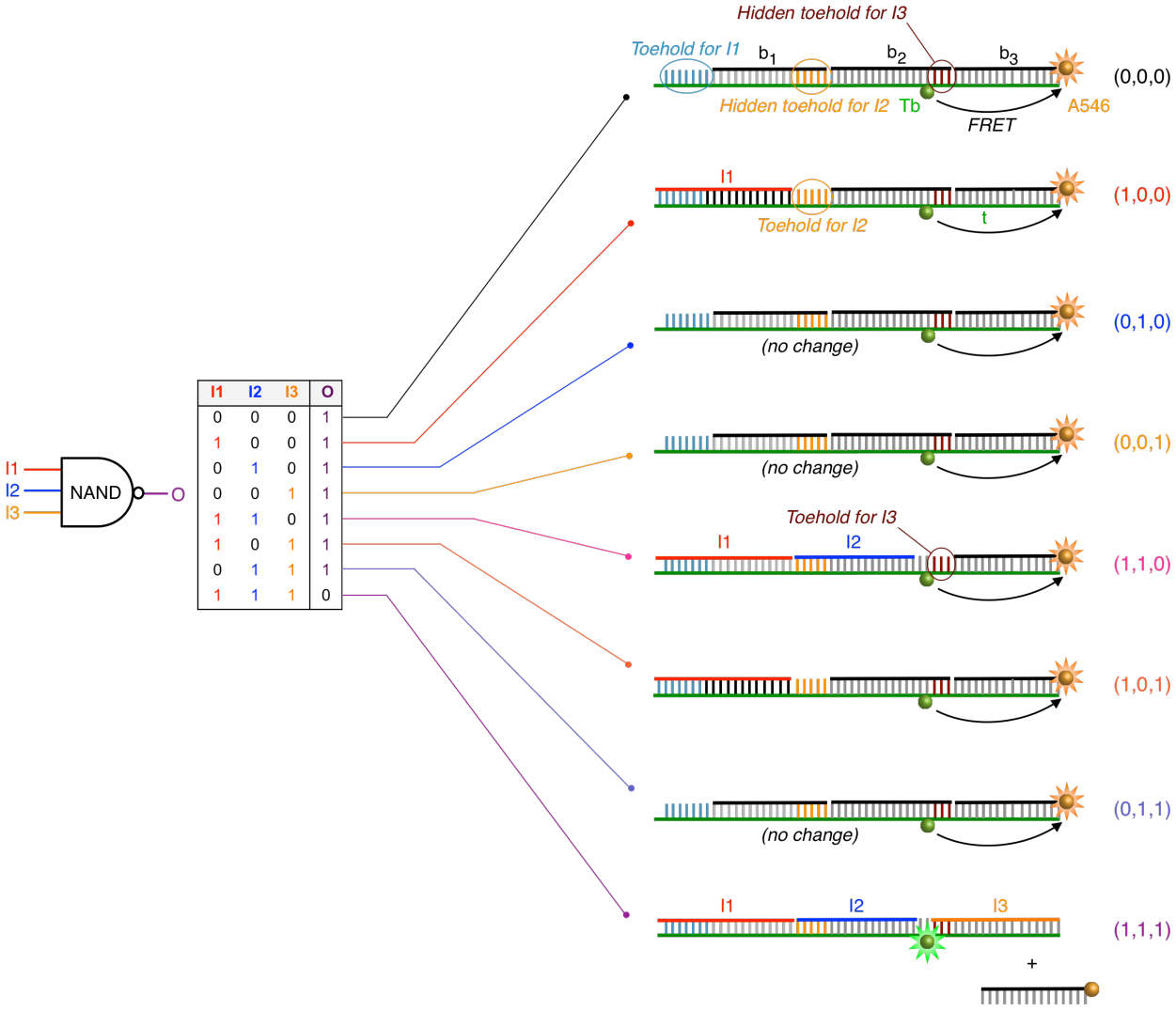

Figure S11. Truth table and DNA structures for a three-input NAND gate. The template (t), blocking (b_1, b_2, b_3), and input (I1, I2, I3) oligonucleotides are labeled. Tb and A546 are also labeled. Toeholds for strand displacement by the inputs are circled. Efficient FRET is shown as a solid arrow.

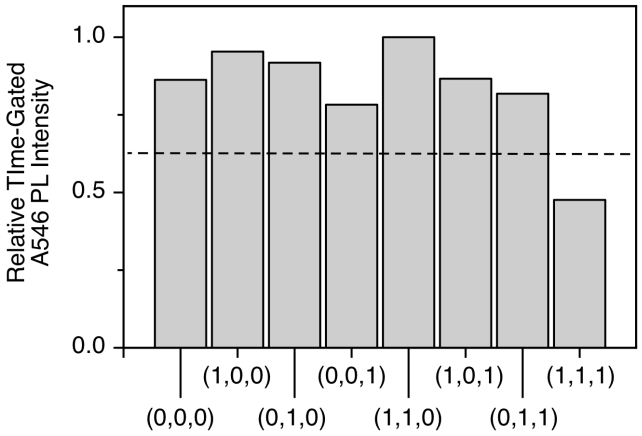

Figure S12. Experimental truth table as the relative time-gated A546 PL intensity when the three-input NAND gate was challenged with different combinations of its three inputs. The "true/false" threshold is shown as the dashed line.

Additional References

1. Thubagere, A. J.; Thachuk, C.; Berleant, J.; Johnson, R. F.; Ardelean, D. A.; Cherry, K. M.; Qian, L. Compiler-Aided Systematic Construction of Large-Scale DNA Strand Displacement Circuits Using Unpurified Components. *Nat. Commun.* **2017,** *8*, 14373.
2. Zhang, D. Y.; Winfree, E. Robustness and Modularity Properties of a Non-Covalent DNA Catalytic Reaction. *Nucleic Acids Res.* **2010,** *38*, 4182-4197.
3. Massey, M.; Ancona, M. G.; Medintz, I. L.; Algar, W. R. Time-Resolved Nucleic Acid Hybridization Beacons Utilizing Unimolecular and Toehold-Mediated Strand Displacement Designs. *Anal. Chem.* **2015,** *87*, 11923-11931.
4. Zhang, D. Y.; Winfree, E. Control of DNA Strand Displacement Kinetics Using Toehold Exchange. *J. Am. Chem. Soc.* **2009,** *131*, 17303-17314.
5. Srinivas, N.; Ouldridge, T. E.; Sulc, P.; Schaeffer, J. M.; Yurke, B.; Louis, A. A.; Doye, J. P.; Winfree, E. On the Biophysics and Kinetics of Toehold-Mediated DNA Strand Displacement. *Nucleic Acids Res.* **2013,** *41*, 10641-10658.
6. Seeling, G.; Soloveichik, D; Zhang, D.Y.; Winfree, E. Enzyme-Free Nucleic Acid Logic Circuits. *Science*, **2006**, *314*, 1585-1588.